ELSEVIER

Physica A 231 (1996) 20–48

PHYSICA A

Scaling and universality in animate and inanimate systems

H.E. Stanley [a,*], L.A.N. Amaral [a], S.V. Buldyrev [a], A.L. Goldberger [b], S. Havlin [a,c], H. Leschhorn [a], P. Maass [a], H.A. Makse [a], C.-K. Peng [a,b], M.A. Salinger [d], M.H.R. Stanley [a], G.M. Viswanathan [a]

[a] *Center for Polymer Studies and Department of Physics, Boston University, Boston, MA 02215, USA*
[b] *Cardiovascular Division, Harvard Medical School, Beth Israel Hospital, Boston, MA 02215 USA*
[c] *Minerva Center and Department of Physics, Bar-Ilan University, Ramat Gan, Israel*
[d] *School of Management, Boston University, Boston, MA 02215, USA*

Abstract

We illustrate the general principle that in biophysics, econophysics and possibly even city growth, the conceptual framework provided by scaling and universality may be of use in making sense of complex statistical data. Specifically, we discuss recent work on DNA sequences, heartbeat intervals, avalanche-like lung inflation, urban growth, and company growth. Although our main focus is on data, we also discuss statistical mechanical models.

1. Introduction

The twin pillars of scaling and universality support much of our current conceptualization on the general subject of just how complex systems formed of interacting subunits should behave [1]. These pillars were constructed a quarter century ago by scientists interested in the behavior of a system near its critical point. Progress was made possible by a remarkable combination of experiment and phenomenological theory. To help conceptualize the problem, the Ising model came to play a key role, and indeed most of the ideas that emerged were tested on this model system.

The Ising model is defined to be a set of classical spins localized on the sites of a lattice. Each spin is a one-dimensional object that can point either "up" or "down." The ferromagnetic Ising interaction is particularly simple: If two neighboring spins are parallel (both up or both down), then there is a negative contribution to the energy. Hence the lowest energy of the entire system will be the configuration in which all the

* Corresponding author.

PII S0378-4371(96)00086-6

spins in the system are parallel. The Ising model can be regarded as a crude model of a ferromagnet if we think of the classical spins as representing the constituent microscopic moments comprising the ferromagnet.

Studies of the Ising model reveal a remarkable feature. If one tunes a "control parameter" – the temperature T – then one finds that, at a certain critical value T_c, spins remarkably far apart have orientations that are strongly correlated. Such correlations do not lend themselves to a ready explanation. The reason is that normally in physics modelling "you get out what you put in". In the case of the Ising model, we "put in" an interaction that extends a finite distance. Magically, we "get out" a correlation that spreads an *infinite* distance. How does this happen?

Our intuition tells us that the correlation $C(r)$ between subunits separated by a distance r should decay exponentially with r – for the same reason the value of money stored in ones mattress decays exponentially with time (each year it loses a constant fraction of its worth). Thus $C(r) \sim e^{-r/\xi}$, where ξ is termed the correlation length – the characteristic length scale above which the correlation function is negligibly small. Experiments and also calculations on mathematical models confirm that correlations do indeed decay exponentially so long as the system is not exactly *at* its critical point, where the rapid exponential decay turns into a long-range power-law decay of the form $C(r) \sim r^{-\eta}$, where η is called a critical exponent [1]. If correlations decay with a power-law form, we say the system is "scale free" since there is no characteristic scale associated with a simple power law.

Critical exponents, such as η, are found empirically to depend most strongly upon the system dimension and on the general symmetry properties of the constituent subunits, and not on other details of the system under investigation. We understand power law decay as arising primarily from the multiplicity of interaction paths that connect two spins in dimensions larger than one [2]. Exact enumeration methods take into account exactly the contributions of such paths – up to a maximum length that depends on the strength of the computer used and the patience of the investigator. To obtain quantitative results, the hierarchy of exact results is extrapolated to infinite order. In some sense, although the correlation along each path *decreases* exponentially with the length of the path, the number of such paths *increases* exponentially. The "gently decaying" power-law correlation emerges as the victor in this competition between the two warring exponential effects.

Cyril Domb, Michael Fisher, the late Walter Marshall and their colleagues pioneered such exact enumeration approaches in the 1970s. Among the results emerging from their efforts was a calculation of the scaling equation of state in a magnetic field [3]. A remarkable feature of much work is that the system studied does not perfectly mirror the conditions of the model definition, yet the scaling equation of state measured conforms almost perfectly to the calculated result [3]. How can that be?

The quick answer is one word: "universality". The word universality connotes the fact that quite disparate systems behave in a remarkably similar fashion near their respective critical points – simply because near their critical points what matters most is not the details of the microscopic interactions but rather the nature of the "paths along which

order is propagated". The experiments in question are essentially two-dimensional, and the component "magnetic moments" have sufficient anisotropy in their interactions that when acting collectively they behave as one-dimensional classical spins. Hence the experimental system mirrors a two-dimensional Ising model!

At one time, it was imagined that the "scale-free" case was relevant to only a fairly narrow slice of physical phenomena [1]. However, the range of systems that apparently display power law correlations has increased dramatically in recent years, ranging from base pair correlations in DNA [4], lung inflation [5,6] and interbeat intervals of the human heart [7] to complex systems involving large numbers of interacting subunits that display "free will," such as govern city growth [8] and even economics [9–13]. The principle of universality seems to be reflected in the empirical fact that quite different systems can have remarkably similar critical exponents – perhaps the "interaction paths" between the constituent subunits dominate the observed cooperative behavior more than the detailed properties of the subunits themselves.

The purpose of this lecture is to describe a few examples of recent progress in applying concepts of modern statistical physics to systems of relevance to biology, medicine, urban growth, and economics.

2. Scaling in biology and medicine: A brief survey

In the last decade, it was realized that some biological systems have no characteristic length or time scale, i.e., they have fractal – or, more generally, self-affine – properties [14–16]. However, the fractal properties in different biological systems, have quite different nature, origin, and appearance. In some cases, it is the geometrical shape of a biological object itself that exhibits obvious fractal features, while in other cases the fractal properties are more "hidden" and can only be perceived if data are studied as a function of time or mapped onto a graph in some special way. After an appropriate mapping, such a graph may resemble a mountain landscape, with jagged ridges of all length scales from very small bumps to enormous peaks (see Fig. 1). Mathematically, these landscapes can be quantified in terms of fractal concepts such as self-affinity.

In contrast to compact objects, fractal objects have a very large *surface* area. In fact, they are composed almost entirely of "surface." This observation explains why fractals are ubiquitous in biology, where surface phenomena [16] are of crucial importance.

Lungs exemplify this feature (see Fig. 2). The surface area of a human lung is as large as a tennis court. The mammalian lung is made up of self-similar branches with many length scales, which is the defining attribute of a fractal surface. The efficiency of the lung is enhanced by this fractal property, since with each breath oxygen and carbon dioxide have to be exchanged at the lung surface. The structure of the bronchial tree has been quantitatively analyzed using fractal concepts [15–17,5]. In particular, fractal geometry could explain the power law decay of the average diameter of the bronchial tube with the generation number, in contrast to the classical model which predicts an exponential decay [18].

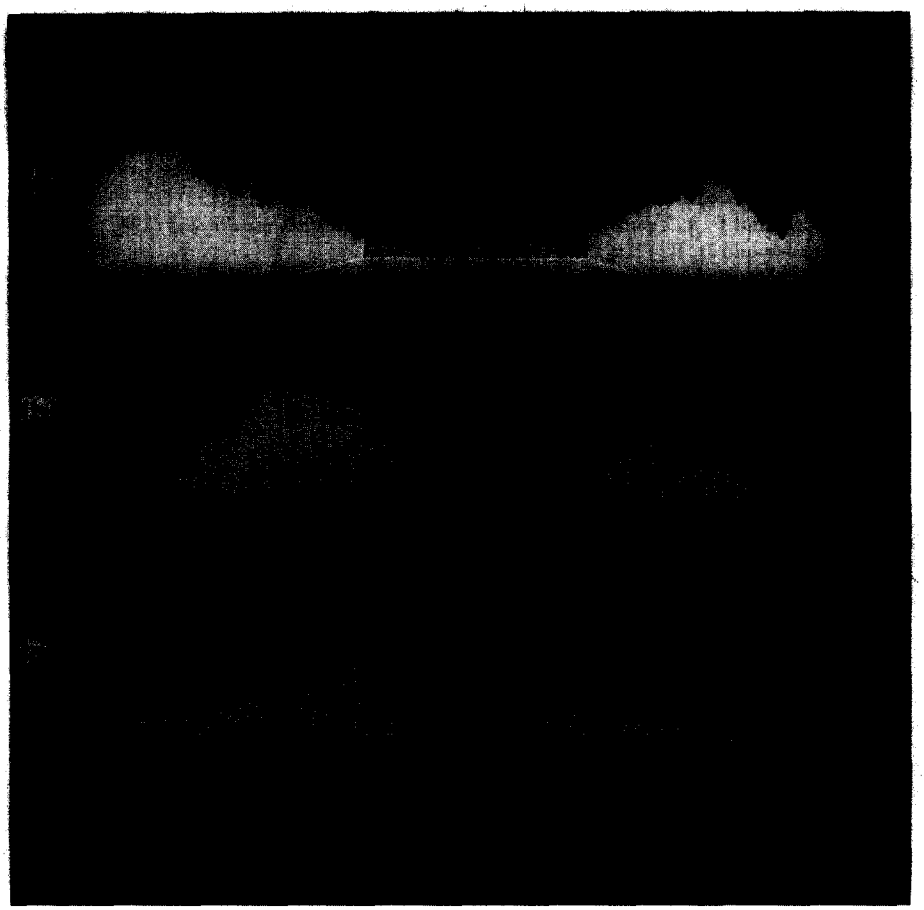

Fig. 1. The DNA walk representation for the rat embryonic skeletal myosin heavy chain gene ($\alpha = 0.63$). At the top the entire sequence is shown. In the middle the solid box shown in the top is magnified. At the bottom the solid box shown in the middle is magnified. The statistical self-similarity of these plots is consistent with the existence of a scale-free or fractal phenomenon which we call a fractal landscape. Note that one must magnify the segment by different factors along the ℓ (horizontal) direction and the y (vertical) direction; since F has the same units (dimension) as y, these magnification factors M_ℓ and M_y (along ℓ and y directions respectively) are related to the scaling exponent α by the simple relation $\alpha = \log(M_y)/\log(M_\ell)$ [e.g., from top to middle, $\log(M_y)/\log(M_\ell) = \log(2.07)/\log(3.2) = 0.63$].

Not only the geometry of the respiratory tree is described by fractal geometry, but also the time-dependent features of inspiration. Specifically, Suki et al. [5] studied airway opening in isolated dog lungs. During constant flow inflations, they found that the lung volume changes in discrete jumps (Fig. 2), and that the probability distribution function of the relative size x of the jumps, $\Pi(x)$, and that of the time intervals t between these jumps, $\Pi(t)$, follow a power law over nearly two decades of x and t with exponents of 1.8 and 2.7, respectively. To interpret these findings, they developed a branching airway model in which airways, labeled ij, are closed with a uniform distribution of opening threshold pressures P. When the "airway opening" pressure P_{ao}

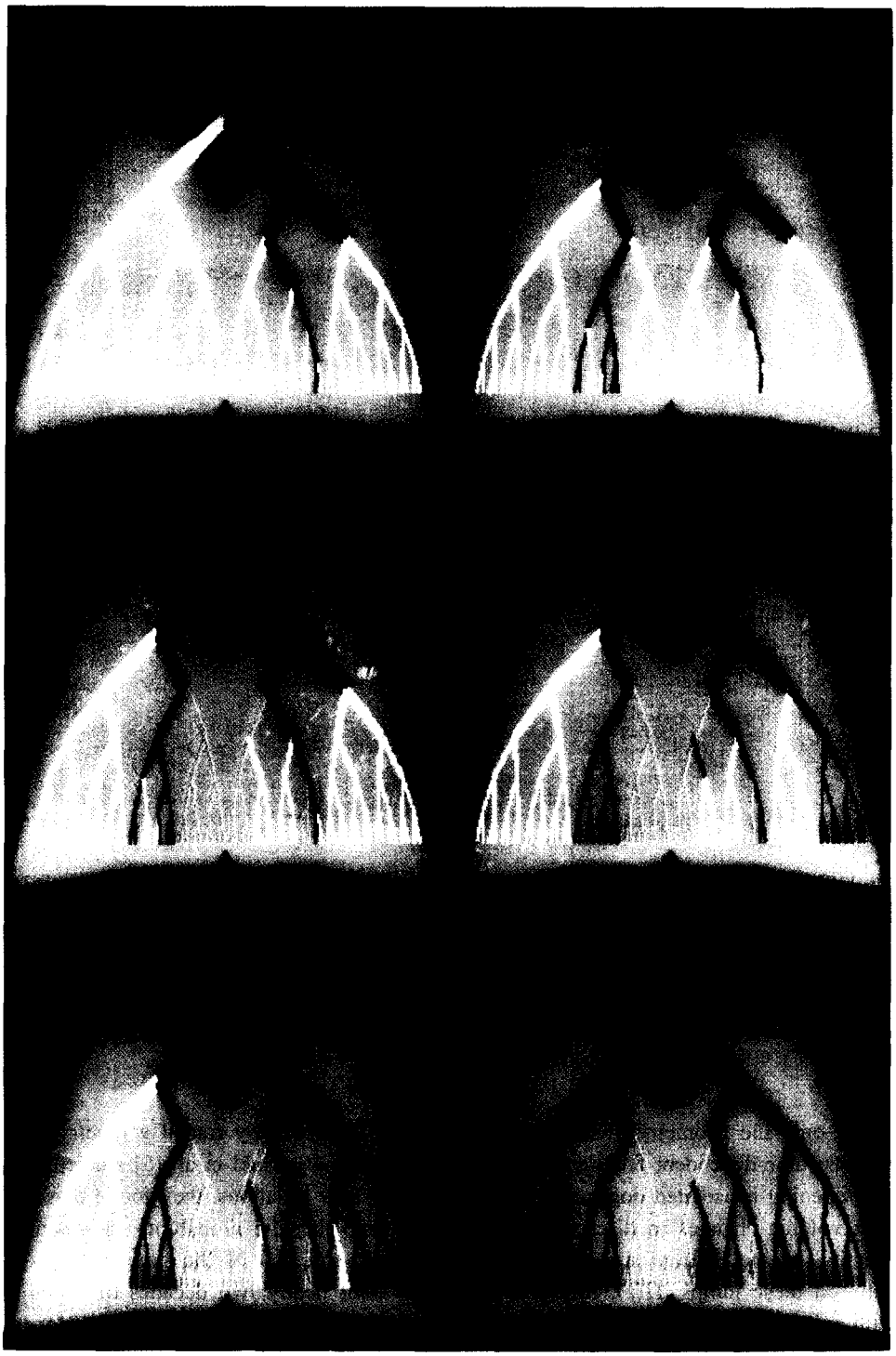

Fig. 2.

exceeds P_{ij} of an airway, that airway opens along with one or both of its daughter branches if $P_{ij} < P_{ao}$ for the daughters. Thus, the model predicts "avalanches" of airway openings with a wide distribution of sizes, and the statistics of the jumps agree with those $\Pi(x)$ and $\Pi(t)$ measured experimentally. They concluded that power-law distributions, arising from avalanches triggered by threshold phenomena, govern the recruitment of terminal airspaces.

A second example is the arterial system which delivers oxygen and nutrients to all the cells of the body. For this purpose blood vessels must have fractal properties [19,20]. The diameter distribution of blood vessels ranging from capillaries to arteries follows a power-law distribution which is one of the main characteristics of fractals. Sernetz et al. [21] have studied the branching patterns of arterial kidney vessels. They analyzed the mass-radius relation and found that it can be characterized by fractal geometry, with fractal dimensions between 2 and 2.5. Similarly, the branching of trees and other plants, as well as root systems have a fractal nature [22]. Moreover, the size distribution of plant-supported insects was found to be related to the fractal distribution of the leaves [23].

One of the most remarkable examples of a fractal object is the surface of a cauliflower, where every little head is an "almost" exact reduced copy of the whole head formed by intersecting Fibonacci spirals of smaller heads, which in turn consist of spirals of smaller and smaller heads, up to the fifth order of hierarchy. West and Goldberger were first to describe such a "Fibonacci fractal" in the human lung [15]. (For a general review of fractals in physiology and medicine see also Ref. [15].)

Considerable interest in the biological community has also arisen from the possibility that neuron shape can be quantified using fractal concepts. For example, Smith et al. [24] studied the fractal features of vertebrate central nervous system neurons in culture and found that the fractal dimension is increased as the neuron becomes more developed. Caserta et al. [25] showed that the shapes of quasi-two-dimensional retinal neurons can be characterized by a fractal dimension d_f. They found for fully developed neurons in vivo, $d_f = 1.68 \pm 0.15$, and suggest that the growth mechanism for neurite outgrowth bears a direct analogy with the growth model called *diffusion limited aggregation* (DLA). The branching pattern of retinal vessels in a developed human eye is also similar to DLA [20]. The fractal dimension was estimated to be about 1.7, in good agreement with DLA for the case of two dimensions. For an alternative model for retinal growth see [26].

Fig. 2. The dynamic mechanism responsible for filling the lung involves "avalanches" or "bursts" of air that occur in all sizes – instead of an exponential distribution, one finds a power-law distribution [5]. The underlying cause of this scale-free distribution of avalanches is the fact that every airway in the lung has its own threshold below which it is not inflated. Shown here is a diagram of the development of avalanches in the airways during airway opening. At first, almost all airways whose threshold value is smaller than the external pressure (red) are closed. Then the airway opening pressure increases until a second threshold is exceeded, and as a result all airways further up the tree whose thresholds are smaller become inflated (green). The airway opening pressure is successively increased until third, fourth, and fifth thresholds are exceeded (yellow, brown, and blue). The last threshold to be exceeded results in filling the airways colored violet; we notice that this last avalanche opens up over 25% of the total lung volume, thereby significantly increasing the total surface area available for gas exchange. After [5].

The DLA-type model governing viscous fingering may also serve to resolve the age-old paradox "Why doesn't the stomach digest itself?" [27]. Indeed, the concentration of hydrochloric acid in the mammalian stomach after each meal is sufficient to digest the stomach itself, yet the gastric epithelium normally remains undamaged in this harsh environment. One protective factor is gastric mucus, a viscous secretion of specialized cells, which forms a protective layer and acts as a diffusion barrier to acid. Bicarbonate ion secreted by the gastric epithelium is trapped in the mucus gel, establishing a gradient from pH 1–2 at the lumen to pH 6–7 at the cell surface. The puzzle, then, is how hydrochloric acid, secreted at the base of gastric glands by specialized parietal cells, traverses the mucus layer to reach the lumen without acidifying the mucus layer. Bhaskar et al. [27] resolved this puzzle by experiments that demonstrate the possibility that flow of hydrochloric acid through mucus involves viscous fingering – the phenomenon that occurs when a fluid of lower viscosity is injected into a more viscous one (see Fig. 3). Specifically, Bhaskar et al. demonstrated that injection of hydrochloric acid through solutions of pig gastric mucin produces fingering patterns which are strongly dependent on pH, mucin concentration, and acid flow rate. Above pH 4, discrete fingers are observed, while below pH 4, hydrochloric acid neither penetrates the mucin solution nor forms fingers. These in vitro results suggest that hydrochloric acid secreted by the gastric gland can penetrate the mucus gel layer (pH 5–7) through narrow fingers, whereas hydrochloric acid in the lumen (pH 2) is prevented from diffusing back to the epithelium by the high viscosity of gastric mucus gel on the luminal side.

Yet another example of DLA-type growth is bacterial colony spread on the surface of agar (gel with nutrient) plates [28]. Vicsek et al. [29] studied bacterial colony growth on a strip geometry which results in a self-affine surface (see Fig. 13.19 in [30]). They calculated the roughness exponent α for this surface and found $\alpha = 0.78 \pm 0.07$. The interfacial pattern formation of the growth of bacterial colonies was studied systematically by Ben-Jacob et al. [31]. They demonstrated that bacterial colonies can develop a pattern similar to morphologies in diffusion-limited growth observed in solidification and electro-chemical deposition. These include fractal growth, dense-branching growth, compact growth, dendritic growth and chiral growth. The results indicate that the interplay between the micro level (individual bacterium) and the macro level (the colony) play a major role in selecting the observed morphologies similar to those found in nonliving systems.

Another example of fractal interface appears in ecology, in the problem of the territory covered by N diffusing particles [32] (see Fig. 4). As seen from the figure, the territory initially grows with the shape of a disk with a relatively smooth surface until it reaches a certain size, at which point the surface becomes increasingly rough. This phenomenon may have been observed by Skellam [33] who plotted contours delineating the advance of the muskrat population and noted that initially the contours were smooth but at later times they became rough (see Fig. 1 in [33]).

Other biological contexts in which fractal scaling seems to be relevant are the relation between brain size and body weight [34], between bone diameter and bone length [35],

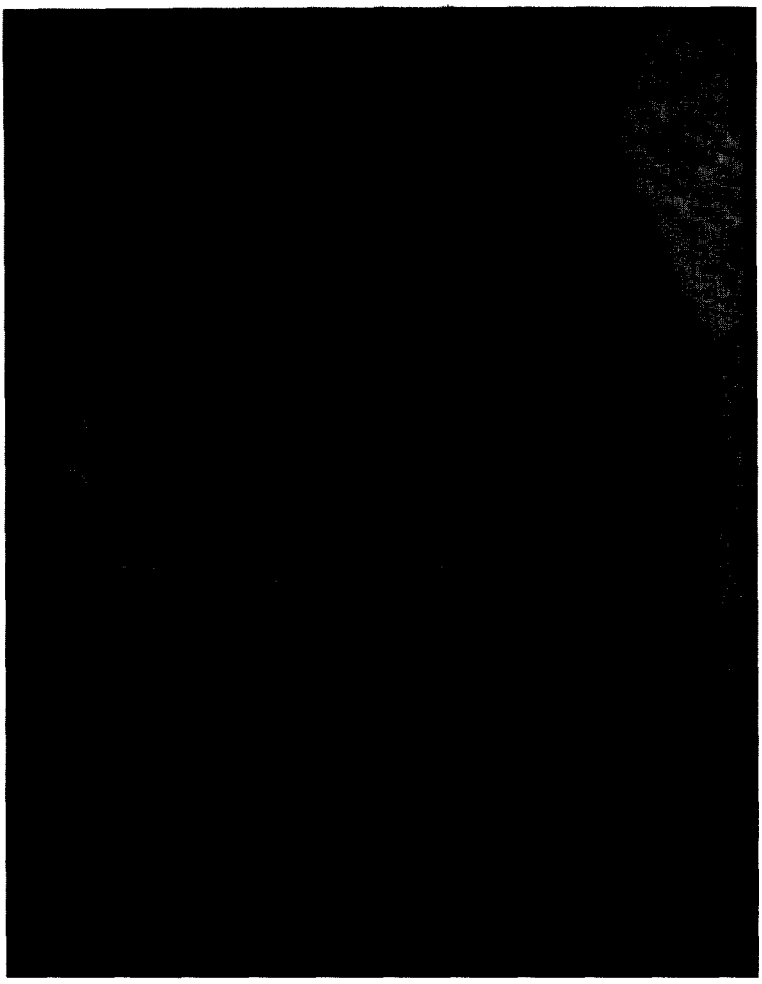

Fig. 3. Viscous fingers reflect the complex interface that develops when one fluid is pumped through another of higher viscosity. Shown is the formation of such viscous fingers or channels when hydrochloric acid is injected into solutions of gastric mucin. These channels may confine the acid and direct it to the lumen, thus protecting the gastric mucosa from acidification and ulceration; when the gastric glands contract, acid is ejected under high enough pressure to form viscous fingers. After [27].

between muscle force and muscle mass [35], and between an organism's size and its rate of producing energy and consuming food [36].

3. Scaling in DNA base pair sequences

The role of genomic DNA sequences in coding for protein structure is well known [37]. The human genome contains information for approximately 100 000 different proteins, which define all inheritable features of an individual. The genomic

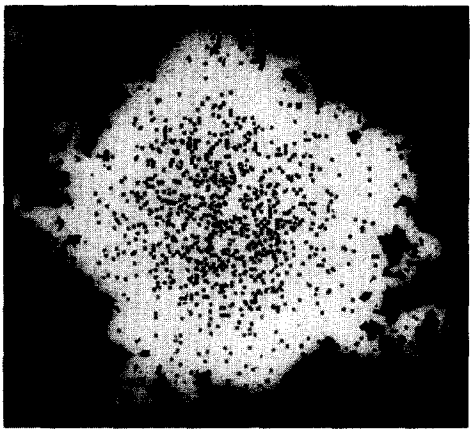

Fig. 4. Snapshots at successive times of the territory covered by N random walkers for the case $N = 500$ for a sequence of times. Note the roughening of the disc surface as time increases. The roughening is characteristic of the experimental findings for the diffusive spread of a population [33]. After [32], courtesy of P. Trunfio.

sequence is likely the most sophisticated information database created by nature through the dynamic process of evolution. Equally remarkable is the precise transformation of information (duplication, decoding, etc.) that occurs in a relatively short time interval.

The building blocks for coding this information are called *nucleotides*. Each nucleotide contains a phosphate group, a deoxyribose sugar moiety and either a *purine* or a *pyrimidine base*. Two purines and two pyrimidines are found in DNA. The two purines are adenine (A) and guanine (G); the two pyrimidines are cytosine (C) and thymine (T).

In the genomes of high eukaryotic organisms only a small portion of the total genome length is used for protein coding (as low as 3% in the human genome). The segments of the chromosomal DNA that are spliced out during the formation of a mature mRNA are called *introns* (for intervening sequences). The coding sequences are called *exons* (for expressive sequences).

The role of introns and intergenomic sequences constituting large portions of the genome remains unknown. Furthermore, only a few quantitative methods are currently available for analyzing information which is possibly encrypted in the noncoding part of the genome.

One interesting question that may be asked by statistical physicists would be whether the sequence of the nucleotides A, C, G, and T behaves like a one-dimensional "ideal gas", where the fluctuations of density of certain particles obey Gaussian law, or if there exist long-range correlations in nucleotide content (as in the vicinity of a critical point). These result in domains of all sizes with different nucleotide concentrations. Such domains of various sizes were known for a long time but their origin and statistical properties remain unexplained. A natural language to describe heterogeneous

DNA structure is long-range correlation analysis, borrowed from the theory of critical phenomena [1].

In order to study the scale-invariant long-range correlations of a DNA sequence, we first introduced a graphical representation of DNA sequences, which we term a *fractal landscape* or *DNA walk* [4]. For the conventional one-dimensional random walk model [38], a walker moves either "up" [$u(i) = +1$] or "down" [$u(i) = -1$] one unit length for each step i of the walk. For the case of an uncorrelated walk, the direction of each step is independent of the previous steps. For the case of a correlated random walk, the direction of each step depends on the history ("memory") of the walker.

One definition of the DNA walk is that the walker steps "up" if a pyrimidine (C or T) occurs at position i along the DNA chain, while the walker steps "down" if a purine (A or G) occurs at position i (see Fig. 1). The question we asked was whether such a walk displays only short-range correlations (as in a Markov chain) or long-range correlations (as in critical phenomena and other scale-free "fractal" phenomena – see Fig. 1). A different type of DNA walk was introduced earlier by Azbel [39].

There have also been attempts to map DNA sequence onto multi-dimensional DNA walks [40,41]. However, recent work [42] indicates that the original purine–pyrimidine rule provides the most robust results, probably due to the purine–pyrimidine chemical complementarity.

An important statistical quantity characterizing any walk is the root mean square fluctuation $F(\ell)$ about the average of the displacement of a quantity $\Delta y(\ell)$ defined by $\Delta y(\ell) \equiv y(\ell_0 + \ell) - y(\ell_0)$, where

$$y(\ell) \equiv \sum_{i=1}^{\ell} u(i). \tag{1}$$

If there is no characteristic length (i.e., if the correlations were "infinite-range"), then fluctuations will also be described by a power law

$$F(\ell) \sim \ell^{\alpha} \tag{2}$$

with $\alpha \neq \frac{1}{2}$. The exponent α is the self-similarity parameter mentioned above and therefore is directly related to long-range correlations in the sequence.

The fact that data for intron-containing and intergenic (i.e., noncoding) sequences are linear on this double logarithmic plot confirms that $F(\ell) \sim \ell^{\alpha}$. A least-squares fit produces a straight line with slope α substantially larger than the prediction for an uncorrelated walk, $\alpha = \frac{1}{2}$, thus providing direct experimental evidence for the presence of long-range correlations.

Fig. 5 shows the DFA exponent $\alpha(\ell)$ for the nine sequenced chromosomes of *Saccharomyces cerevisiae* using the purine–pyrimidine rule and the hydrogen bond energy rule. Note that although the landscapes look quite different, the LRC exponent $\alpha(\ell)$ is very similar for different chromosomes. For $\ell < 1000$ bp the different chromosomes have almost identical $\alpha(\ell)$. This similarity indicates that the correlation properties of

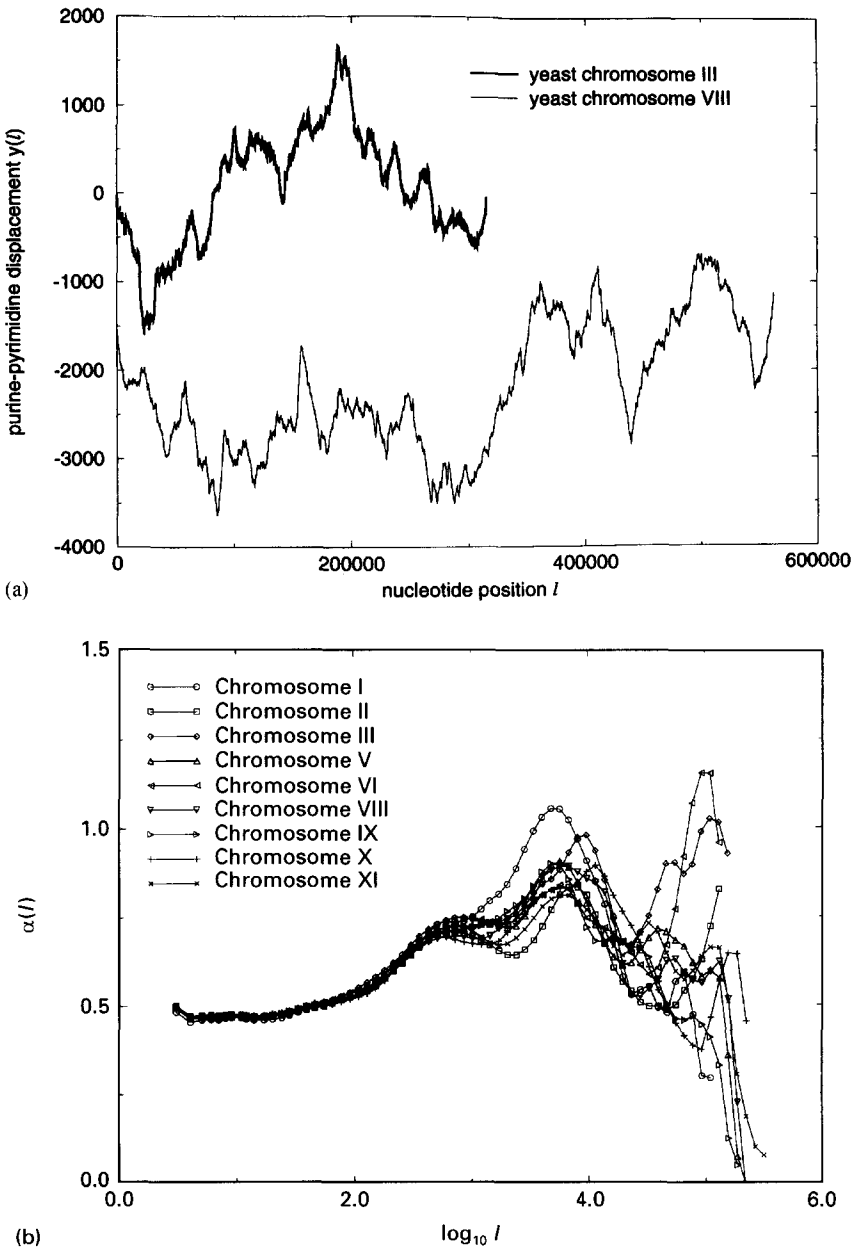

Fig. 5. (a) DNA walk for yeast chromosomes III and VIII. (b) Local exponent $\alpha(\ell)$ measured on length scale ℓ. Note that even though the two chromosomes have dramatically different landscapes, the $\alpha(\ell)$ functions are similar.

the different chromosomes are almost the same for $\ell < 1000$ bp. Note also how the first couple of peaks in $\alpha(\ell)$ roughly coincide for the different chromosomes in Fig. 7(b). This indicates that the nine chromosomes have similar patch sizes, because peaks in $\alpha(\ell)$ correspond to characteristic patch sizes.

4. Scaling in nonstationary heartbeat time series

Clinicians often describe the normal activity of the heart as "regular sinus rhythm." But in fact cardiac interbeat intervals normally fluctuate in a complex, apparently erratic manner [44] [Fig. 6(a)]. This highly irregular behavior has recently motivated researchers [45, 46] to apply time series analyses that derive from statistical physics, especially methods for the study of critical phenomena where fluctuations at all length (time) scales occur. These studies show that under healthy conditions, interbeat interval time series exhibit long-range power-law correlation reminiscent of physical systems near a critical point [47, 1]. Furthermore, certain disease states may be accompanied by alterations in this scale-invariant (fractal) correlation property.

The work in Ref. [7] is based on the digitized electrocardiograms of beat-to-beat heart rate fluctuations recorded with an ambulatory (Holter) monitor. The time series obtained by plotting the sequential intervals between beat i and beat $i + 1$, denoted by $B(i)$, typically reveals a complex type of variability [Fig. 6(a)]. The mechanism underlying such fluctuations appears to be related primarily to countervailing neuroautonomic inputs. The nonlinear interaction (competition) between the two branches of

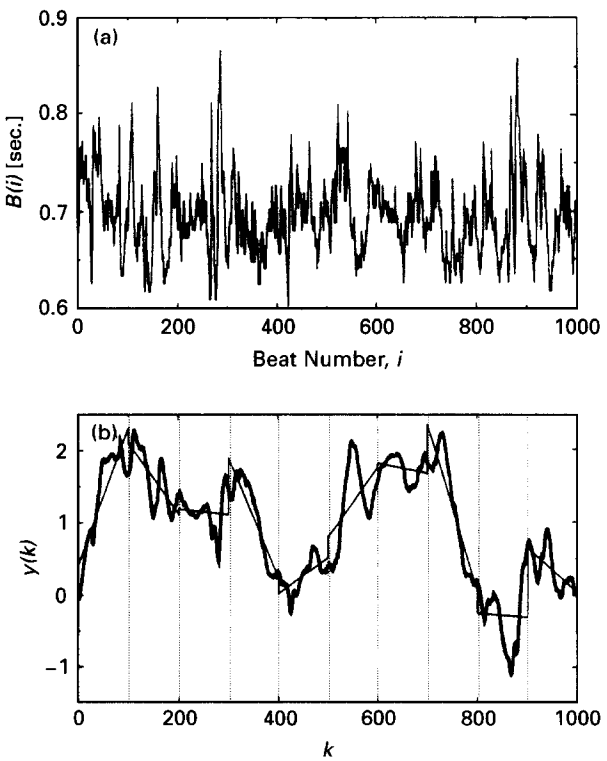

Fig. 6. (a) The interbeat interval time series $B(i)$ of 1000 beat. (b) The integrated time series: $y(k) = \Sigma_{i=1}^{k}[B(i) - B_{av}]$, where $B(i)$ is the interbeat interval shown in (a). The vertical dotted lines indicate box of size $n = 100$, the solid straight lines segments are the estimated "trend" in each box by least-squares fit.

the autonomic nervous system is the postulated mechanism for the type of erratic heart rate variability recorded in healthy subjects [44,48].

An immediate problem facing researchers applying time series analysis to interbeat interval data is that the heartbeat time series is often highly nonstationary. To overcome this problem, we introduced a modified fluctuation analysis of a random walk – termed *detrended fluctuation analysis* (DFA) [49] – to the analysis of physiological data. The advantages of DFA over conventional methods (e.g., spectral analysis and Hurst analysis) are that it permits the detection of long-range correlations embedded in a seemingly nonstationary time series, and also avoids the spurious detection of apparent long-range correlations that are an artifact of nonstationarity.

To illustrate the DFA algorithm, we use the interbeat time series shown in Fig. 6(a) as an example. Briefly, the interbeat interval time series (of total length N) is first integrated, $y(k) = \sum_{i=1}^{k}[B(i) - B_{av}]$, where $B(i)$ is the ith interbeat interval and B_{av} is the average interbeat interval. Next the integrated time series is divided into boxes of equal length, n. In each box of length n, a least-squares line was fit to the data (representing the *trend* in that box) [Fig. 6(a)]. The y coordinate of the straight line segments is denoted by $y_n(k)$. Next we detrend the integrated time series, $y(k)$, by subtracting the local trend, $y_n(k)$, in each box. The root-mean-square fluctuation of this integrated and detrended time series is calculated by

$$F(n) = \sqrt{\frac{1}{N}\sum_{k=1}^{N}[y(k) - y_n(k)]^2}. \tag{3}$$

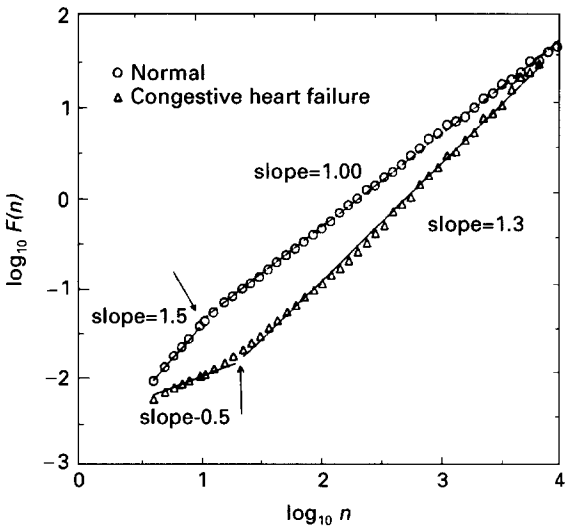

Fig. 7. Plot of $\log F(n)$ versus $\log n$ for two very long interbeat interval time series (~24 h). The circles are for a healthy subject while the triangles are from a subject of congestive heart failure. Arrows indicate "crossover" points in scaling.

Fig. 7 compares the DFA analysis of representative 24 h interbeat interval time series of a healthy subject (○) and a patient with congestive heart failure (△). Notice that for large time scales (asymptotic behavior), the healthy subject shows almost perfect power-law scaling over two decades ($20 \leqslant n \leqslant 10\,000$) with $\alpha = 1$ (i.e., $1/f$ noise) while for the pathologic data set $\alpha \approx 1.3$ (closer to Brownian noise). This result is consistent with our previous finding that there is a significant difference in the long-range scaling behavior between healthy and diseased states [45,46].

5. Scaling in urban growth patterns

Predicting urban growth is important for the challenge it presents to theoretical frameworks for cluster dynamics [50–52]. Recently, the model of diffusion limited aggregation (DLA) [53] has been applied to describe urban growth [50], and results in tree-like dendritic structures which have a core or "central business district" (CBD). The DLA model predicts that there exists only one large fractal cluster that is almost perfectly screened from incoming "development units" (people, capital, resources, etc.), so that almost all the cluster growth occurs in the extreme peripheral tips. In a recent work [8] an alternative model to DLA that better describes the morphology and the area distribution of systems of cities, as well as the scaling of the urban perimeter of individual cities, has been developed. The results agree both qualitatively and quantitatively with actual urban data. The resulting growth morphology can be understood in terms of the effects of interactions among the constituent units forming a urban region, and can be modeled using the correlated percolation model in the presence of a gradient.

In the model one takes into account the following points:

(i) Urban data on the population density $\rho(r)$ of actual urban systems are known to conform to the relation [54] $\rho(r) = \rho_0 e^{-\lambda r}$, where r is the radial distance from the CBD situated at the core, and λ is the density gradient. Therefore, in our model the development units are positioned with an occupancy probability $p(r) \equiv \rho(r)/\rho_0$ that behaves in the same fashion as is known experimentally.

(ii) In actual urban systems, the development units are not positioned at *random*. Rather, there exist *correlations* arising from the fact that when a development unit is located in a given place, the probability of adjacent development units increases naturally – i.e., each site is not independently occupied by a development unit, but is occupied with a probability that depends on the occupancy of the neighborhood.

In order to quantify these ideas, we consider the *correlated* percolation model [55–57]. In the limit where correlations are so small as to be negligible [58], a site at position r is occupied if the occupancy variable $u(r)$ is smaller than the occupation probability $p(r)$; the variables $u(r)$ are uncorrelated random numbers. To introduce correlation among the variables, we convolute the uncorrelated variables $u(r)$ with a suitable power-law kernel [57], and define a new set of random variables $\eta(r)$ with long-range power-law correlations that decay as $r^{-\alpha}$, where $r \equiv |r|$. The assumption of power-law interactions is motivated by the fact that the "decision" for a development

unit to be placed in a given location decays gradually with the distance from an occupied neighborhood. The correlation exponent α is the only parameter to be determined by empirical observations.

To discuss the morphology of a system of cities generated in the present model, we show in Figs. 8 and 9 our simulations of correlated urban systems for a fixed value of the density gradient λ, and for different degree of correlations. The correlations have the effect of agglomerating the units around a urban area. In the simulated systems the largest city is situated in the core, which is regarded as the attractive center of the city, and is surrounded by small clusters or "towns". The correlated clusters are nearly compact near their centers and become less compact near their boundaries, in qualitative agreement with empirical data on actual large cities such as Berlin, Paris and London (see, e.g., Refs. [50, 59]).

So far, we have argued how correlations between occupancy probabilities can account for the irregular morphology of towns in a urban system. As can be seen in Fig. 10, the towns surrounding a large city like Berlin are characterized by a wide range of sizes. We are interested in the laws that quantify the town size distribution $N(A)$, where A is the area occupied by a given town or "mass" of the agglomeration, so we calculate the actual distribution of the areas of the urban settlements around Berlin and London, and find that for both cities, $N(A)$ follows a power law.

This new result of a power-law area distribution of towns, $N(A)$, can be understood in the context of our model. Insight into this distribution can be developed by first noting that the small clusters surrounding the largest cluster are all situated at distances r from the CBD such that $p(r) < p_c$ or $r > r_f$. Therefore, we find $N(A)$, the cumulative area distribution of clusters of area A, to be

$$N(A) \equiv \int_0^{p_c} n(A, p)\, dp \sim A^{-(\tau+1/d_f \nu)}. \tag{4}$$

Here, $n(A, p) \sim A^{-\tau} g(A/A_0)$ is defined to be the average number of clusters containing A sites for a given p *at a fixed distance* r, and $\tau = 1 + 2/d_f$. Here, $A_0(r) \sim |p(r) - p_c|^{-d_f \nu}$ corresponds to the maximum typical area occupied by a cluster situated at a distance r from the CBD, while $g(A/A_0)$ is a scaling function that decays rapidly (exponentially) for $A > A_0$. The exponent $\nu = \nu(\alpha)$ is defined by $\xi(r) \sim |p(r) - p_c|^{-\nu}$, where $\xi(r)$ is the connectedness length that represents the mean linear extension of a cluster at a distance $r > r_f$ from the CBD.

Fig. 8. Simulations of urban systems for different degree of correlations. Here, the urban areas are red, and the external perimeter or urban boundary of the largest cluster connected to the CBD is light green. In all the figures, we fix the value of the density gradient to be $\lambda = 0.009$. (a) and (b) Two different examples of interactive systems of cities for correlation exponents $\alpha = 0.6$ and $\alpha = 1.4$, respectively. The development units are positioned with a probability that decays exponentially with the distance from the core. The units are located not randomly as in percolation, but rather in a correlated fashion depending on the neighboring occupied areas. The correlations are parametrized by the exponent α. The strongly correlated case corresponds to small α ($\alpha \to 0$). When $\alpha > d$, where d is the spatial dimension of the substrate lattice ($d = 2$ in our case), we recover the uncorrelated case. Notice the tendency to more compact clusters as we increase the

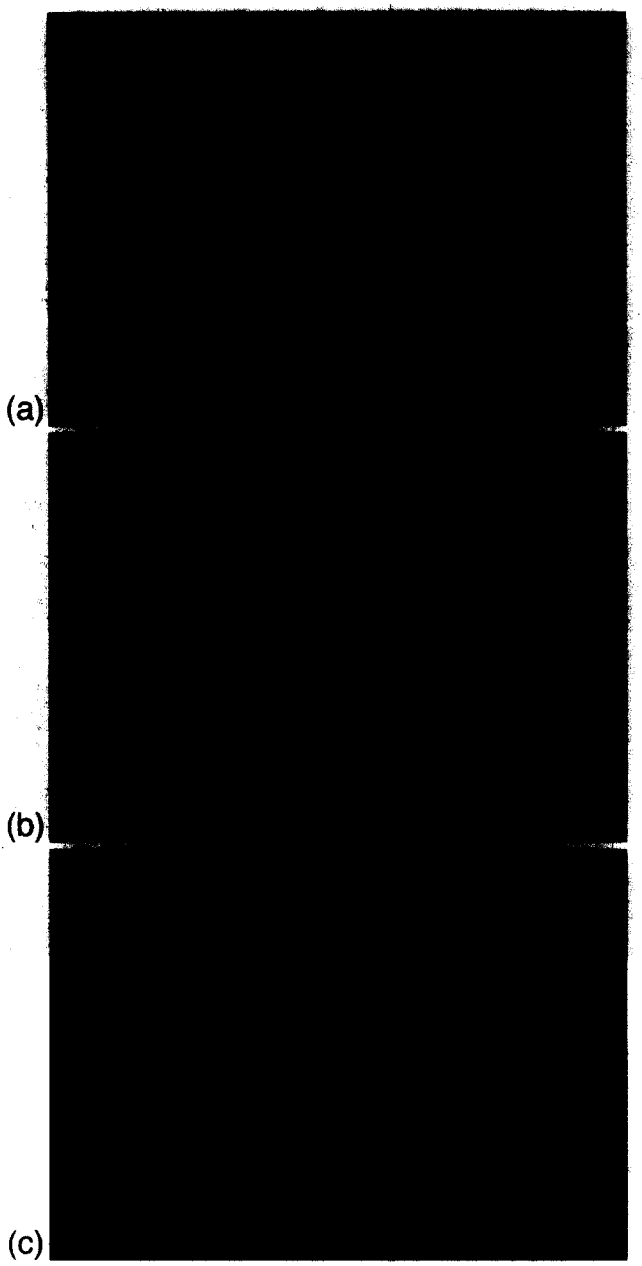

Fig. 8. continued.
degree of correlations ($\alpha \to 0$). (c) As a zeroth-order approximation, one might imagine the morphology predicted in the extreme limit whereby development units are positioned at *random*, rather than in the correlated way. The results for this crude approximation of a noninteractive (uncorrelated) system of cities clearly display a drastically different morphology than found from data on real cities. The noninteractive limit looks unrealistic in comparison with real cities, for the lack of interactions creates a urban area characterized by many small towns spread loosely around the core.

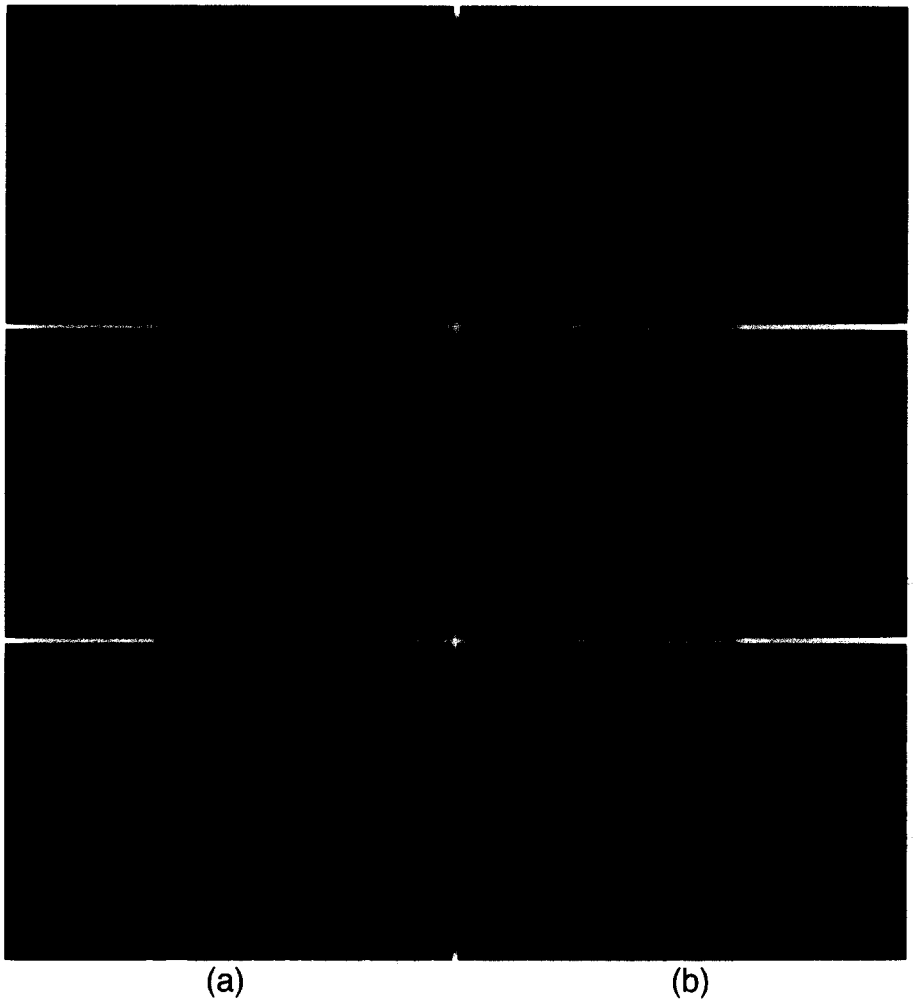

Fig. 9. The population distributions of Berlin and surrounding town from the years 1875, 1920, and 1945 (left column, top to bottom) resemble those in an urban growth model based on correlated percolation (right column).

6. Modeling DNA evolution and economics

The question arises whether these long-range correlations in noncoding DNA sequences and the entire chromosomes are the simple consequence of patches of DNA with different nucleotide concentration [60]. Indeed, how can power-law correlations arise in the one-dimensional system such as DNA, where correlations should decay exponentially with distance between nucleotides in analogy with spins of one-dimensional Ising Model? One of the possible answers to this question is the duplication–mutation model of DNA evolution suggested by Li [61].

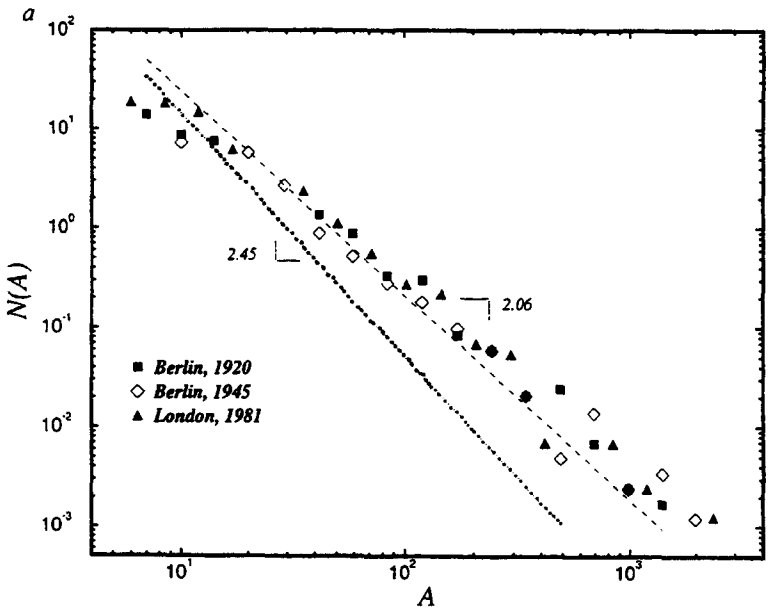

Fig. 10. Log-log plot of the area distribution $N(A)$ of the actual towns around Berlin and London. We first digitize the empirical data. Then we count the number of towns that are covered by A sites, putting the result in logarithmically spaced bins (of size 1.2^k, with $k = 1, 2, \ldots, 15$), and averaging over the size of the bin. A power-law is observed for the area distributions of both urban systems. The dotted line shows the predictions of our model for the uncorrelated case (slope = 2.45), while the dashed line gives results for the strongly correlated case (slope = 2.06). Note that the area distributions for both cities agree much better with the strongly correlated case ($\alpha \to 0$).

In this model the time axes serves as an additional spatial dimension which connects distant segments of DNA which have been developed from a single ancestor.

The model is based on two assumptions both of which are biologically motivated:

(1) Every nucleotide can mutate with a certain probability.

(2) Every nucleotide can be duplicated or deleted with a certain probability.

The first phenomenon is known as point mutation which can be caused by random chemical reactions such as methylation [62]. Second phenomenon often happens in the process of cell division (mitosis and myosis) when pairs of sister chromosomes exchange segments of their DNA (genetic crossover). If the exchanging segments are of identical length the duplication does not happen. However, if two segments differ in length by n nucleotides, the chromosome that acquires larger segment obtains an extra sequence of length n which is identical to its neighbor, while another chromosome loses this sequence. Thus a tandem repeat of length n appears on one of the sister chromosomes. In many cases duplications can be more evolutionary advantageous than deletions. In this case lengthy tandemly repeated regions will emerge from a single repeat. For simplicity we will start with a model similar to the original model of Li [61] which neglects deletions and deals with duplication of single nucleotides ($n = 1$). Next we will discuss the implications of deletions.

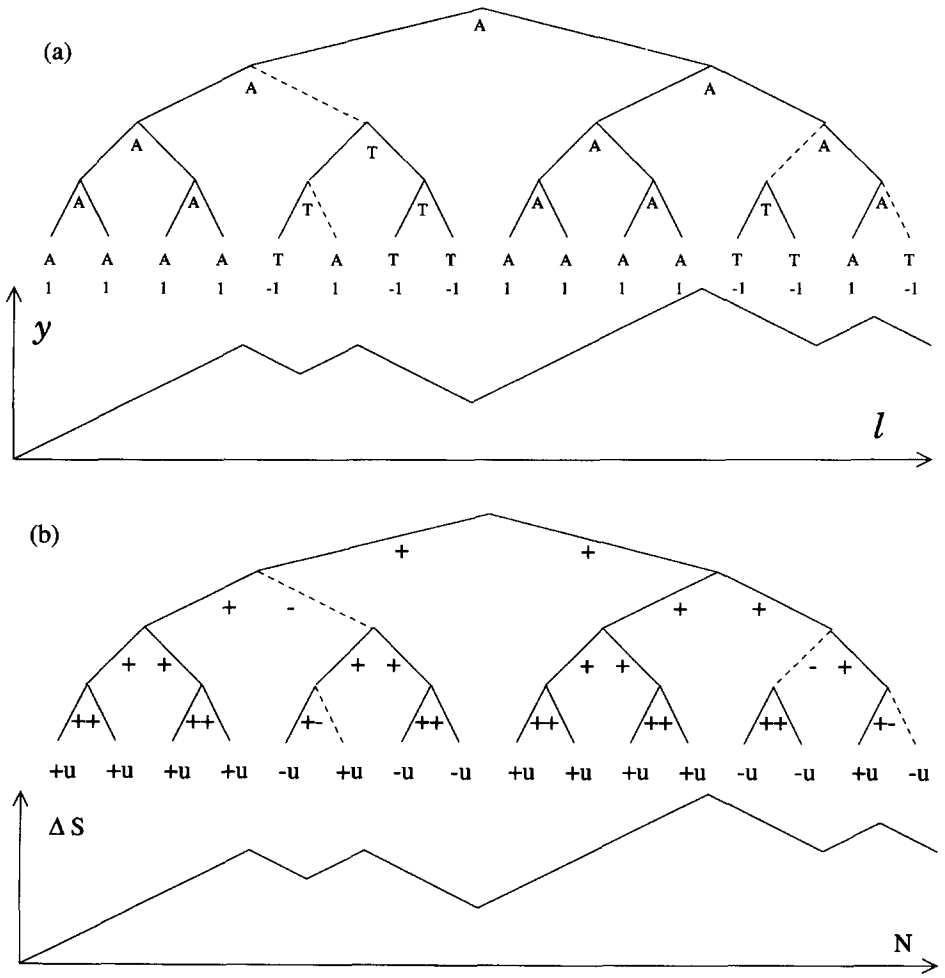

Fig. 11. (a) Schematic representation of the most simple example of duplication–mutation process proposed by W. Li. Originally the sequence consists of only one nucleotide A. At any time step, represented by a certain horizontal level of the tree each nucleotide duplicates and some of them mutate with probability $p_m \ll 1$. Mutation events are shown by dashed lines. For simplicity we assume only two nucleotides A and T . The DNA walk representation of the obtained sequence is shown below the tree. (b) Analogous plot for the structure of a firm. Dashed lines correspond to modifications of the "bosses" decisions by lower level management. To total change in sales can be calculated by adding changes u_i of each branch of a firm listed below the tree.

Schematically, this model can be illustrated by Fig. 11. Each level of the tree-like structure represents one step of evolution process during which each nucleotide always duplicates and with probability p_m also mutates. For simplicity we assume only two types of nucleotides a and b (say purine versus pyrimidine) each of which is represented by a step up or down in the DNA walk representation. After k steps, this process will lead to a sequence of 2^k nucleotides which is represented by DNA landscape, shown

below. The total excess of purines over pyrimidines

$$\Delta y = \sum_{i=1}^{2^k} u_i, \tag{5}$$

is equal to the difference in heights of the starting and the ending points of the walk. In the following we compute explicitly the correlation

$$C(\ell) = \langle u_i u_{i+\ell} \rangle \tag{6}$$

between nucleotides which are ℓ nucleotides apart from each other along the resulting sequence. The reason why the correlations are now long-range is obvious. Indeed, the nucleotides which are $\ell = 2^{k'}$ apart from each other in space are only $2k'$ apart from each other in time, since they are both descendants of one common ancestor $k' = \log_2 \ell$ generations before. The correlation decay exponentially with k' and hence as a power law of ℓ.

Simple calculations yield

$$\langle u_i u_{i+\ell} \rangle = (1 - 2p_m)^{2k'} = \ell^{2\ln(1-2p_m)/\ln 2}. \tag{7}$$

Thus

$$\gamma = -\frac{2\ln(1 - 2p_m)}{\ln 2}, \tag{8}$$

and, using (5),

$$\alpha = 1 - \frac{|\ln(1 - 2p_m)|}{\ln 2}. \tag{9}$$

Note that $\alpha = 1$ when $p_m = 0$ and α becomes $\frac{1}{2}$ when $p_m > \frac{1}{2}(1 - 1/\sqrt{2})$.

In general, when the deletions might occur with some probability $p_d < \frac{1}{2}$, the number of descendants of one common ancestor grows as $z^{k'}$ where $z = 2(1 - p_d)$ and k' is the number of generations.

Thus, replacing $\ln 2$ by $\ln z$ in the denominators of expressions (8) and (9), we get

$$\gamma = \frac{2\ln(1 - 2p_m)}{\ln(2 - 2p_d)}, \qquad \alpha = 1 - \frac{2\ln(1 - 2p_m)}{\ln(2 - 2p_d)}. \tag{10}$$

More rigorous but less evident approach of recursion relations among levels of the tree lead to the same analytical results – see Eqs. (8)–(10).

Similar arguments can be applied for computation of α in more complex situations when more than one nucleotide can duplicate and all four types of nucleotides are present, however simple analytical results in this case are not available.

In summary, the model suggested by Li may lead under reasonable assumptions to the experimentally observed values of α which are in the range between 0.5 and 1. In the next section, we show how this model can be applied to the study of an economic system.

7. Scaling in economics

Another seemingly unrelated phenomenon is the behavior of industrial firm sales or their employment. We have studied the dependence of the fluctuations of the annual firm growth rates on the initial size of the firm [11].

Specifically, we studied all US manufacturing publicly traded firms within the years 1975–1991. The data were taken from the Compustat database and all values for sales have been adjusted to 1987 dollars by the GNP price deflator. We define a firm's annual growth rate as $R \equiv S_1/S_0$, where S_0 and S_1 are its sales in two consecutive years.

It is customary to study firm growth on logarithmic scales, so we define $r \equiv \ln(S_1/S_0)$ and $s_0 \equiv \ln S_0$ and calculate the conditional distribution $p(r|s_0)$ of growth rates r with a given initial sales value s_0.

The distribution $p(r|s_0)$ of the growth rates from 1990 to 1991 is shown in Fig. 12(a) for two different values of initial sales. Remarkably, both curves display a simple "tent-shaped" form. The distribution is not Gaussian – as expected from the Gibrat model – but rather is exponential,

$$p(r|s_0) = \frac{1}{\sqrt{2}\sigma(s_0)} \exp\left(-\frac{\sqrt{2}\,|r - \bar{r}(s_0)|}{\sigma(s_0)}\right). \tag{11}$$

The straight lines shown in Fig. 1(a) are calculated from the average growth rate $\bar{r}(s_0)$ and the standard deviation $\sigma(s_0)$ obtained by fitting the data set to Eq. (11).

We also find that the data for *each* annual interval from 1975–1991 fit well to Eq. (11), with only small variations in the parameters $\bar{r}(s_0)$ and $\sigma(s_0)$. To improve the statistics, we therefore calculate the new distribution by averaging all the data from the 16 annual intervals in the database. As shown in Fig. 12(b), the data now scatter much less and the shape is well described by Eq. (11). For this reason, we have also included in the figure data for "volatile" cases, corresponding to sales of only about 2.6×10^5 dollars.

As is apparent from Fig. 12(b), $\sigma(s_0)$ decreases with increasing s_0. We find $\sigma(s_0)$ is well approximated over more than seven orders of magnitude – from sales of less than 10^4 dollars up to sales of more than 10^{11} dollars – by the law

$$\sigma(s_0) = a \exp(-\beta s_0) \; = a S_0^{-\beta}, \tag{12}$$

where $a \simeq 6.66$ and $\beta = 0.15 \pm 0.03$ (Fig. 13).

We performed a parallel analysis for the number of employees, and the corresponding standard deviation is shown in Fig. 13. The data are linear over roughly five orders of magnitude, from firms with only ten employees to firms with almost 10^6 employees. The slope $\beta = 0.16 \pm 0.03$ is the same, within error bars, as that found for sales.

We find that Eqs. (11) and (12) accurately describe three additional indicators of firm growth (Fig. 14): (i) cost of goods sold (with exponent $\beta = 0.16 \pm 0.03$) (ii) assets ($\beta = 0.17 \pm 0.04$) and (iii) property, plant and equipment ($\beta = 0.18 \pm 0.03$).

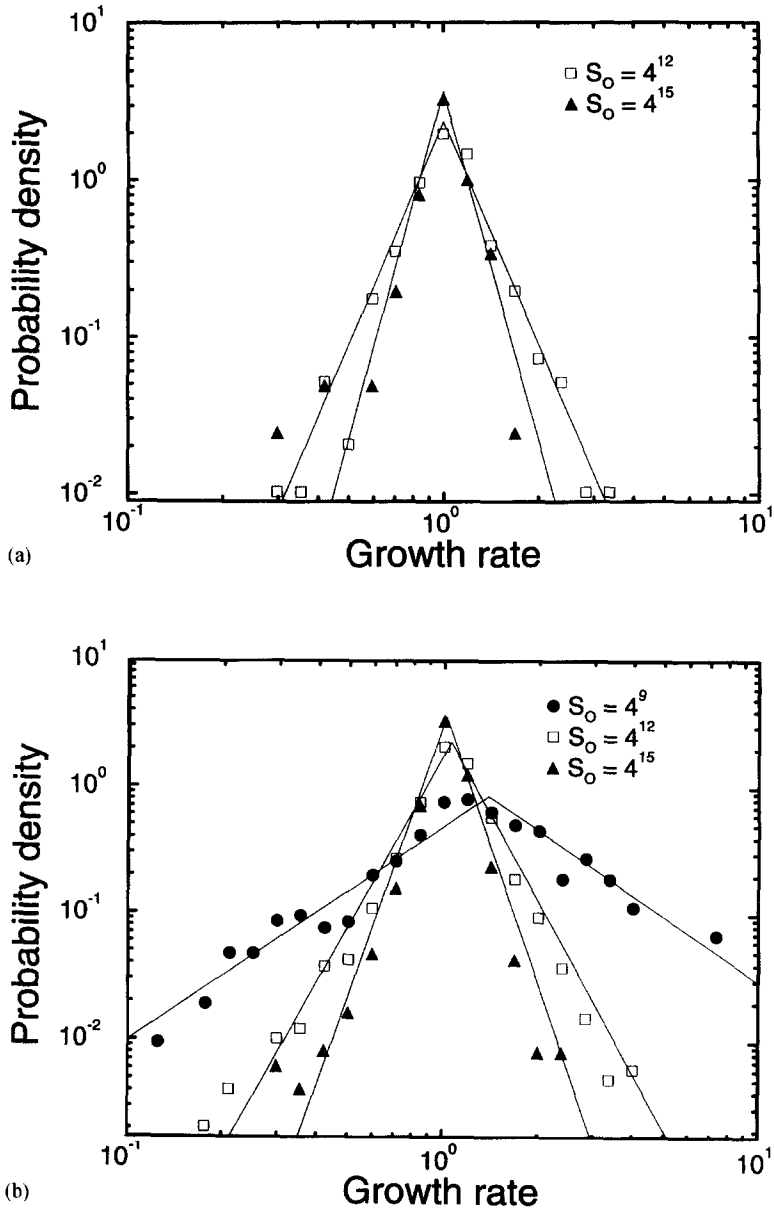

Fig. 12. (a) Probability density $p(r|s_0)$ of the growth rate $r \equiv \ln(S_1/S_0)$ from year 1990 to 1991 for all publicly traded US manufacturing firms in 1994 Compustat with standard industrial classification index of 2000–3999. We examine 1991 because between 1992 and 1994 there are several firms with zero sales that either have gone out of business or are "new technology" firms (developing new products). We show the data for two different bins of initial sales (with sizes increasing by powers of 4): $4^{11.5} < S_0 < 4^{12.5}$ and $4^{14.5} < S_0 < 4^{15.5}$. Within each sales bin, each firm has a different value of R, so the abscissa value is obtained by binning these R values. The solid lines are fits to Eq. (11) using the mean $\bar{r}(s_0)$ and standard deviation $\sigma(s_0)$ calculated from the data. (b) Probability density $p(r|s_0)$ of the annual growth rate, for three different bins of initial sales: $4^{8.5} < S_0 < 4^{9.5}$, $4^{11.5} < S_0 < 4^{12.5}$, and $4^{14.5} < S_0 < 4^{15.5}$. The data were averaged over all 16 1 yr periods between 1975 and 1991. The solid lines are fits to Eq. (11) using the mean $\bar{r}(s_0)$ and standard deviation $\sigma(s_0)$ calculated from all data.

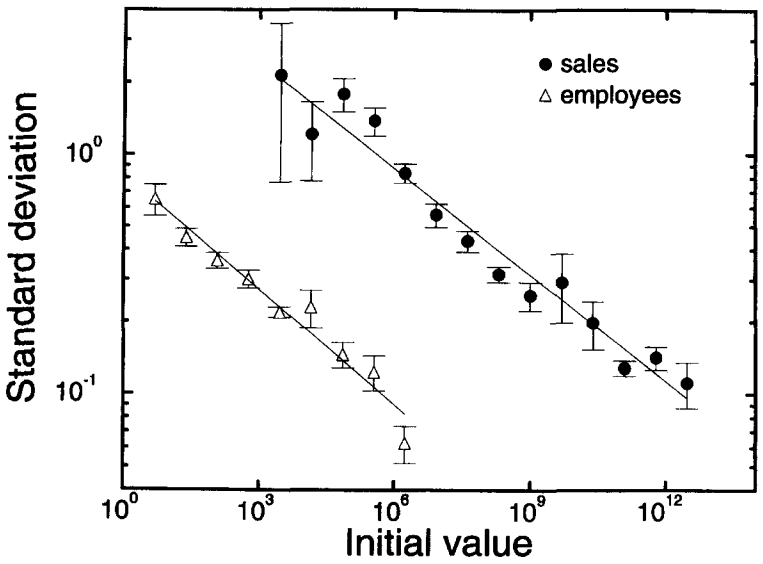

Fig. 13. Standard deviation of the 1 yr growth rates of the sales and of the 1 yr growth rates of the number of employees as a function of the initial values. The solid lines are least-square fits to the data with slopes $\beta = 0.15 \pm 0.03$ for the sales and $\beta = 0.16 \pm 0.03$ for the number of employees. We also show error bars of one standard deviations about each data point. These error bars appear asymmetric since the ordinate is a log scale.

What is remarkable about Eqs.(11) and (12) is that they govern the growth rates of a diverse set of firms. They range not only in their size but also in what they manufacture. The conventional economic theory of the firm is based on production technology, which varies from product to product. Conventional theory does not suggest that the processes governing the growth rate of car companies should be the same as those governing, e.g., pharmaceutical or paper firms. Indeed, our findings are reminiscent of the concept of universality found in statistical physics, where different systems can be characterized by the same fundamental laws, independent of "microscopic" details.

Scaling phenomena of the sort that we have uncovered in the sales and employee distribution functions are sometimes represented graphically by plotting a suitably "scaled" dependent variable as a function of a suitably "scaled" independent variable. If scaling holds, then the data for a wide range of parameter values are said to "collapse" upon a *single* curve. To test the present data for such data collapse, we plot (Fig. 15) the scaled probability density $p_{\mathrm{scal}} \equiv \sqrt{2}\sigma(s_0)p(r|s_0)$ as a function of the scaled growth rates of both sales and employees $r_{\mathrm{scal}} \equiv \sqrt{2}[r - \bar{r}(s_0)]/\sigma(s_0)$. The data collapse upon the single curve $p_{\mathrm{scal}} = \exp(-|r_{\mathrm{scal}}|)$. Our results for (i) cost of goods sold, (ii) assets, and (iii) property, plant and equipment are equally consistent with such scaling.

The power-law dependence of $\sigma(S_0)$ on S_0 may have its origin in the internal structure of each firm. In the simplest approach, one would assume that the sales S_0 of a

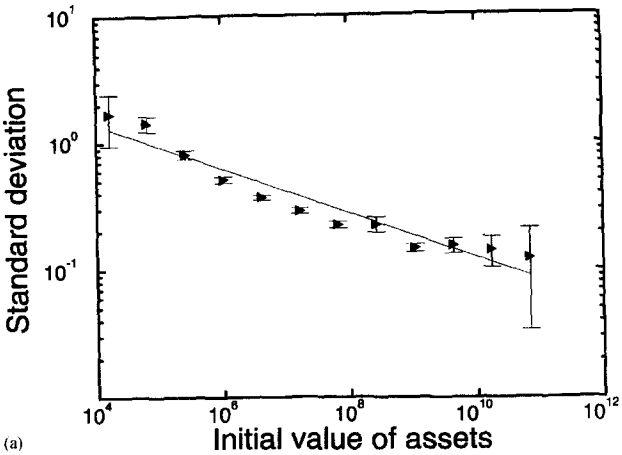

(a)

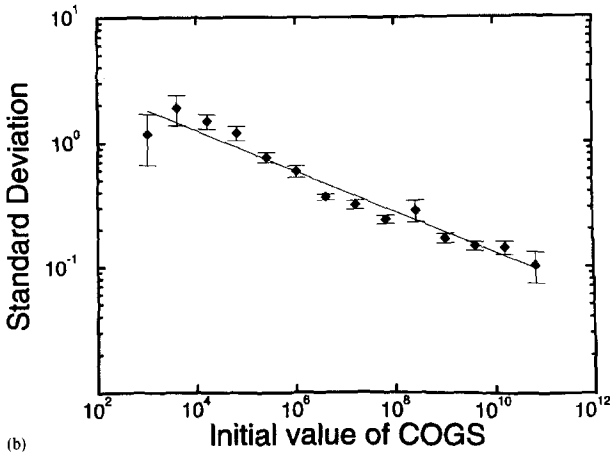

(b)

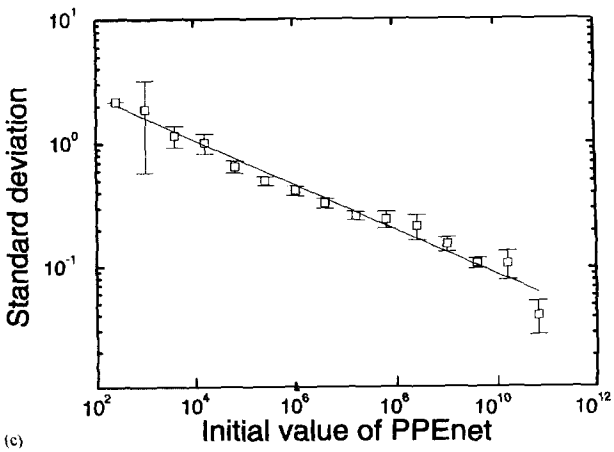

(c)

Fig. 14. Power-law dependence of standard deviation $\sigma(S)/S$ on initial size S for three quantities: (a) S denotes assets (slope of -0.18), (b) S denotes cost of goods sold (slope of -0.16 and (c) S denotes property, plant, and equipment (slope of -0.18).

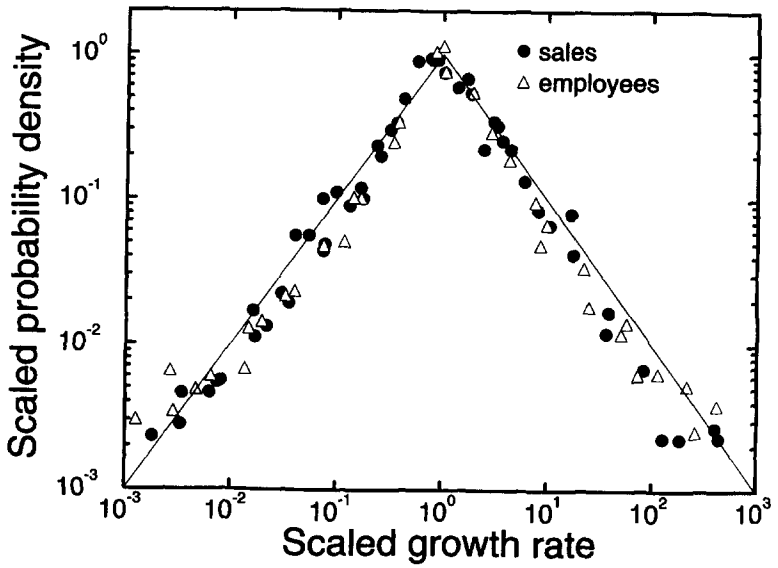

Fig. 15. Scaled probability density $p_{\mathrm{scal}} \equiv 2^{1/2}\sigma(s_0)p(r|s_0)$ as a function of the scaled growth rate $r_{\mathrm{scal}} \equiv 2^{1/2}[r - \bar{r}(s_0)]/\sigma(s_0)$. The values were rescaled using the measured values of $\bar{r}(s_0)$ and $\sigma(s_0)$. Also we show the analogous scaled quantities for the number of employees. All the data collapse upon the universal curve $p_{\mathrm{scal}} = \exp(-|r_{\mathrm{scal}}|)$ as predicted by Eqs. (11) and (12).

given company result from N independent units

$$S_0 = \sum_{i=1}^{N} \xi_i. \tag{13}$$

If the unit sales ξ_i have a typical average $\langle \xi \rangle = S_0/N$ and an annual variation u_i independent of s_0, then the annual change in sales is

$$\Delta S = \sum_{i=1}^{N} u_i. \tag{14}$$

In analogy with a random walk, $\sigma(S_0)$ would grow as $\sqrt{N}$ or since N is proportional to S_0 as $\sqrt{S_0}$, thus giving $\alpha = \frac{1}{2}$ so that $\beta = 1 - \alpha = \frac{1}{2}$. The much larger value of α that we find ($\alpha \approx 0.8$) indicates the presence of strong correlations among the firm's units. We can model this phenomena by considering the tree-like hierarchical organization of a typical firm (see Fig. 11(b)). The root of the tree represents the head of the company, whose policy is passed to the level beneath, and so on, until finally the units in the lowest level take action. Each of these units has an average sales value $\langle \xi \rangle = S_0/N$ and a corresponding typical fluctuation u. The number of links connecting the levels will vary from level to level, but there is a value z which represents a certain average number of links. Then the number of units N is equal to z^k, where k is the number of levels.

What are the consequences of this simple model? Let us first assume that the head of the firm suggests a policy that could result in changing the sales of each unit by an amount u. If this policy is propagated through the hierarchy without any modifications, then the change in sales is simply $\Delta S = N_u = S_0 u/\langle \xi \rangle$. Accordingly, $\alpha = 1$, so $\beta = 1 - \alpha = 0$.

More realistically, the policy of the head can be modified (undergo "mutation") at each level of the firm management with a small probability p_m. Each unit is not only influenced by the policy of the head but also by other (external and internal) factors. An example is that different levels have different types of information. Managers at each level might deviate from decisions made higher up in the tree if other information suggests to them that another action is appropriate. Another reason for a modification of the policy is organizational failure, due either to poor communication or disobedience. For these reasons, we assume that each manager follows his supervisor's policy with a probability Π, while with probability $(1 - \Pi)$ imposes an *opposite policy* for his subunits, i.e., he decreases the sales by an amount u instead of increasing them, or vice versa. Hence the sales of the entire firm becomes a random variable with a standard deviation that can be explicitly computed using recursion relations among the levels of the tree (see Fig. 11(b)). The result is $\sigma^2(S_0) = u^2[4z p_m(1 - p_m)(y^k - z^k)/(y - z) + y^n]$, where $y = z^2(1 - 2p_m)^2$ and $k = \ln(S_0/\langle \xi \rangle)/\ln z$. For large k, the model predicts $\alpha = 1 - |\ln(1 - 2p_m)|/\ln(z)$ if $z > 1/(1 - 2p_m)^2$ and $\alpha = \frac{1}{2}$ otherwise [see Eq. (9)].

Remarkably, the hierarchical structure of the company (Fig. 11(b)) can be mapped exactly onto the diagram of the DNA mutations and duplications (Fig. 11(a)). Each level of the firm hierarchy corresponds to one generation of repeat family and each modification of the head decision by the lower level management corresponds to a mutation. Note that the $\sigma(S_0)$ for firm sales is exactly $F(\ell)$ for DNA sequences.

Our central results, Eqs. (11) and (12), constitute a test that any accurate theory of the firm must pass, and support the possibility [9] that the scaling laws used to describe complex but inanimate systems comprised of many interacting particles (as occurs in many physical systems) may be usefully extended to describe complex but animate systems comprised of many interacting subsystems (as occurs in economics).

Acknowledgements

We are grateful to many individuals, including M.E. Matsa, S.M. Ossadnik, and F. Sciortino, for major contributions to those results reviewed here that represent collaborative research efforts. We also wish to thank C. Cantor, C. DeLisi, M. Frank-Kamenetskii, A.Yu. Grosberg, G. Huber, I. Labat, L. Liebovitch, G.S. Michaels, P. Munson, R. Nossal, R. Nussinov, R.D. Rosenberg, J.J. Schwartz, M. Schwartz, E.I. Shakhnovich, M.F. Shlesinger, N. Shworak, and E.N. Trifonov for valuable discussions. Partial support was provided by the National Science Foundation, National

Institutes of Health (Human Genome Project), the G. Harold and Leila Y. Mathers Charitable Foundation, the National Heart, Lung and Blood Institute, the National Aeronautics and Space Administration, the Israel–USA Binational Science Foundation, Israel Academy of Sciences, and (to C-KP) by an NIH/NIMH Postdoctoral NRSA Fellowship.

References

[1] H.E. Stanley, Introduction to Phase Transitions and Critical Phenomena (Oxford University Press, Oxford, 1971).
[2] H.E. Stanley and N. Ostrowsky, eds., Correlations and Connectivity: Geometric Aspects of Physics, Chemistry and Biology (Kluwer, Dordrecht, 1990).
[3] S. Milošević and H.E. Stanley, Physical Review B 6 (1972) 986–1001; S. Milošević and H.E. Stanley, Phys. Rev. B 6 (1972) 1002–1008.
[4] C.-K. Peng, S. Buldyrev, A. Goldberger, S. Havlin, F. Sciortino, M. Simons and H.E. Stanley, Nature 356 (1992) 168–171.
[5] B. Suki, A.-L. Barabási, Z. Hantos, F. Peták and H.E. Stanley, Nature 368 (1994) 615–618.
[6] A.-L. Barabási. S.V. Buldyrev, H.E. Stanley and B. Suki, Avalanches in the lung: a statistical mechanical approach, Phys. Rev. Lett. 76 (1996) 2192–2195.
[7] C.K. Peng, S. Havlin, H.E. Stanley and A.L. Goldberger, Chaos 5 (1995) 82–87.
[8] H. Makse, S. Havlin and H.E. Stanley, Nature 377 (1995) 608–612.
[9] R.N. Mantegna and H.E. Stanley, Nature 376 (1995) 46–49.
[10] M.H.R. Stanley, S.V. Buldyrev, S. Havlin, R. Mantegna, M.A. Salinger and H.E. Stanley, Eco. Lett. 49 (1995) 453–457.
[11] M.H.R. Stanley, L.A.N. Amaral, S.V. Buldyrev, S. Havlin, H. Leschhorn, P. Maass, M.A. Salinger and H.E. Stanley, Nature 379 (1996) 804–806.
[12] M.H.R. Stanley, L.A.N. Amaral, S.V. Buldyrev, S. Havlin, H. Leschhorn, P. Maass, R.N. Mantegna, M.A. Salinger and H.E. Stanley, Can Statistical Physics Contribute to the Science of Economics? [Proc. International Conf. on "Future of Fractals"] Fractals 4 (1996).
[13] H.E. Stanley, V. Afanasyev, L.A.N. Amaral, S.V. Buldyrev, A.L. Goldberger, S. Havlin, H. Leschhorn, P. Maass, R.N. Mantegna, C.-K. Peng, P.A. Prince, M.A. Salinger, M.H.R. Stanley and G.M. Viswanathan, Physica A 224 (1996) 302–321.
[14] B.B. Mandelbrot, The Fractal Geometry of Nature (Freeman, San Francisco, 1982).
[15] B.J. West and A.L. Goldberger, J. Appl. Physiol. 60 (1986) 189; B.J. West and A.L. Goldberger, Am. Sci. 75 (1987) 354; A.L. Goldberger and B.J. West, Yale J. Biol. Med. 60 (1987) 421; A.L. Goldberger, D.R. Rigney and B.J. West, Sci. Am. 262 (1990) 42; B.J. West and M.F. Shlesinger, Am. Sci. 78 (1990) 40; B.J. West, Fractal Physiology and Chaos in Medicine (World Scientific, Singapore, 1990); B.J. West and W. Deering, Phys. Reports 254 (1994) 1–100; J.B. Bassingthwaighte, L.S. Liebovitch and B.J. West, Fractal Physiology (Oxford University Press, New York, 1994).
[16] A. Bunde and S. Havlin, eds., Fractals and Disordered Systems (Springer, Berlin, 1991); A. Bunde and S. Havlin, eds., Fractals in Science (Springer, Berlin, 1994); A.-L. Barabasi and H.E. Stanley, Fractal Concepts in Surface Growth (Cambridge University Press, Cambridge, 1995).
[17] M.F. Shlesinger and B.J. West, Phys. Rev. Lett. 67 (1991) 2106.
[18] E.R. Weibel and D.M. Gomez, Science 137 (1962) 577.
[19] A.A. Tsonis and P.A. Tsonis, Perspectives in Biology and Medicine 30 (1987) 355.
[20] F. Family, B.R. Masters and D.E. Platt, Physica D 38 (1989) 98; B.R. Masters, F. Family and D.E. Platt, Biophys. J. (Suppl.) 55 (1989) 575; B.R. Masters and D.E. Platt, Invest. Ophthalmol. Vis. Sci. (Suppl.) 30 (1989) 391.
[21] M. Sernetz, J. Wübbeke and P. Wlczek, Physica A 191 (1992) 13.
[22] H. Takayasu, Fractals in the Physical Sciences (Manchester University Press, Manchester, 1990).
[23] D.R. Morse, Nature 314 (1985) 731.
[24] T.G. Smith, W.B. Marks, G.D. Lange, W.H. Sheriff Jr. and E.A. Neale, J. Neurosci. Methods 27 (1989) 173.

[25] H.E. Stanley, Bull. Am. Phys. Soc. 34 (1989) 716; F. Caserta, H.E. Stanley, W.D. Eldred, G. Daccord, R.E. Hausman and J. Nittmann, Phys. Rev. Lett. 64 (1990) 95; F. Caserta, R.E. Hausman, W.D. Eldred, H.E. Stanley and C. Kimmel, Neurosci. Lett. 136 (1992) 198; F. Caserta, W.D. Eldred, E. Fernandez, R.E. Hausman, L.R. Stanford, S.V. Buldyrev, S. Schwarzer and H.E. Stanley, J. Neurosci. Methods 56 (1995) 133.
[26] D.R. Kayser, L.K. Aberle, R.D. Pochy and L. Lam, Physica A 191 (1992) 17.
[27] K.R. Bhaskar, B.S. Turner, P. Garik, J.D. Bradley, R. Bansil, H.E. Stanley and J.T. LaMont, Nature 360 (1992) 458; R. Bansil, H.E. Stanley and T.J. LaMont, Mucin Biophysics, Annual Rev. Physiology 57 (1995) 635–657.
[28] T. Matsuyama, M. Sugawa and Y. Nakagawa, FEMS Microb. Lett. 61 (1989) 243; H. Fujikawa and M. Matsushita, J. Phys. Soc. Japan 58 (1989) 387; M. Matsushita and H. Fujikawa, Physica A 168 (1990) 498.
[29] T. Vicsek, M. Cserzö and V.K. Horváth, Physica A 167 (1990) 315; S. Matsuura and S. Miyazima, Physica A 191 (1992) 30.
[30] T. Vicsek, Fractal Growth Phenomena, 2nd Ed. (World Scientific, Singapore, 1992).
[31] E. Ben-Jacob, H. Shmueli, O. Shochet and A. Tenenbaum, Physica A 187 (1992) 378; E. Ben-Jacob, A. Tenenbaum, O. Shochet and O. Avidan, Physica A 202 (1994) 1.
[32] H. Larralde, P. Trunfio, S. Havlin, H.E. Stanley and G.H. Weiss, Nature 355 (1992) 423; M.F. Shlesinger, Nature 355 (1992) 396; H. Larralde, P. Trunfio, S. Havlin, H.E. Stanley and G.H. Weiss, Phys. Rev. A 45 (1992) 7128; S. Havlin, H. Larralde, P. Trunfio, J.E. Kiefer, H.E. Stanley and G.H. Weiss, Phys. Rev. A 46 (1992) R-1717; S. Havlin, M. Araujo, H. Larralde, A. Shehter, H.E. Stanley and P. Trunfio, Nuovo Cimento 16 (1995) 1039–1051.
[33] J.G. Skellam, Biometrika 38 (1951) 196.
[34] P.H. Harvey and J.R. Krebs, Science 249 (1990) 140.
[35] R.H. Peters, The Ecological Implications of Body Size (Cambridge University Press, Cambridge, 1983); J.E.I. Hokkanen, J. Theor. Biol. 499 (1956) 499; A.A. Biewener, Science 250 (1990) 1097.
[36] M. Sernetz, B. Gelleri and J. Hofmann, J. Theor. Biol. 187 (1985) 209; R.R. Strathmann, Science 250 (1990) 1091.
[37] J.D. Watson, M. Gilman and J. Witkowski and M. Zoller, Recombinant DNA (Scientific American Books, New York, 1992).
[38] E.W. Montroll and M.F. Shlesinger, The wonderful world of random walks, in: Nonequilibrium Phenomena II. From Stochastics to Hydrodynamics, eds. J.L. Lebowitz and E.W. Montroll (North-Holland, Amsterdam, 1984) pp. 1–121.
[39] M.Ya. Azbel, Phys. Rev. Lett. 31 (1973) 589.
[40] W. Li and K. Kaneko, Europhys. Lett. 17 (1992) 655.
[41] C.L. Berthelsen, J.A. Glazier and M.H. Skolnick, Phys. Rev. A 45 (1992) 8902.
[42] S.M. Ossadnik, S.V. Buldyrev, A.L. Goldberger, S. Havlin, R.N. Mantegna, C.-K. Peng, M. Simons and H.E. Stanley, Biophys. J. 67 (1994) 64.
[43] C.-K. Peng, S.V. Buldyrev, S. Havlin, M. Simons, H.E. Stanley and A.L. Goldberger, Phys. Rev. E 49 (1994) 1685.
[44] A.L. Goldberger, D.R. Rigney and B.J. West, Sci. Am. 262 (1990) 42–49.
[45] C.-K. Peng, J. Mietus, J.M. Hausdorff, S. Havlin, H.E. Stanley and A.L. Goldberger, Phys. Rev. Lett. 70 (1993) 1343–1346.
[46] C.-K. Peng, S.V. Buldyrev, J.M. Hausdorff, S. Havlin, J.E. Mietus, M. Simons, H.E. Stanley and A.L. Goldberger, in: Fractals in Biology and Medicine, eds. T.F. Nonnenmacher, G.A. Losa and E.R. Weibel (Birkhaüser, Basel, 1994), pp. 55–65.
[47] P. Bak, C. Tang and K. Wiesenfeld, Phys. Rev. Lett. 59 (1987) 381–384.
[48] M.N. Lévy, Circ. Res. 29 (1971) 437–445.
[49] C.-K. Peng, S.V. Buldyrev, S. Havlin, M. Simons, H.E. Stanley and A.L. Goldberger, Phys. Rev. E 49 (1994) 1691–1695.
[50] M. Batty and P. Longley, Fractal Cities (Academic Press, San Diego, 1994).
[51] L. Benguigui and M. Daoud, Geog. Analy. 23 (1991) 362–368.
[52] L. Benguigui, J Physica A 219 (1995) 13–26.
[53] T.A. Witten and L.M. Sander, Phys. Rev. Lett. 47 (1981) 1400–1403.
[54] C. Clark, J.R. Stat. Soc. (Series A) 114 (1951) 490–496.
[55] A. Coniglio, C. Nappi, L. Russo and F. Peruggi, J. Phys. A 10 (1977) 205–209.

[56] A. Weinrib, Phys. Rev. B 29 (1984) 387–395.
[57] S. Prakash, S. Havlin, M. Schwartz and H.E. Stanley, Phys. Rev. A 46 (1992) R1724–1727.
[58] J.-F. Gouyet, Physics and Fractal Structures (Springer, Berlin, 1995).
[59] P. Frankhauser, La Fractalité des Structures Urbaines (Collection Villes, Anthropos, Paris, 1994).
[60] S. Karlin and V. Brendel, Science 259 (1993) 677.
[61] W. Li, Phys. Rev. A 43 (1991) 5240–5260; W. Li, Int. J. Bifurcation Chaos 2 (1992) 137–154.
[62] B. Alberts, D. Bray, J. Lewis, M. Raff, K. Roberts and J.D. Watson, Molecular Biology of the Cell, 3rd Ed. (Garland Publishing, New York, 1994).